Remote Sensing of Environment 132 (2013) 1–12

Contents lists available at SciVerse ScienceDirect

Remote Sensing of Environment

journal homepage: www.elsevier.com/locate/rse

Detection of diurnal variation in orchard canopy water content using MODIS/ASTER airborne simulator (MASTER) data

Tao Cheng [a,*], David Riaño [a,b], Alexander Koltunov [a], Michael L. Whiting [a], Susan L. Ustin [a], Jenna Rodriguez [a]

[a] Center for Spatial Technologies and Remote Sensing, Department of Land, Air, and Water Resources, University of California, Davis, CA 95616-8617, USA
[b] Instituto de Economía y Geografía, Centro de Ciencias Humanas y Sociales, Consejo Superior de Investigaciones Científicas (CSIC), Madrid 28006, Spain

ARTICLE INFO

Article history:
Received 10 April 2012
Received in revised form 27 December 2012
Accepted 29 December 2012
Available online xxxx

Keywords:
Canopy water content
NDII
NDVI
MASTER
Diurnal variation
Water stress
BRDF

ABSTRACT

Retrievals of vegetation canopy water content (CWC) from remotely sensed imagery can improve our understanding of the water cycle and help manage irrigation of agricultural crops. Optical remote sensing data can be used to detect seasonal CWC variation but whether they are sensitive enough for detecting diurnal CWC variation remains unknown. This paper investigates whether MODIS/ASTER airborne simulator (MASTER) data can be used to detect diurnal variation in CWC over well irrigated almond and pistachio orchards in the southern San Joaquin Valley of California, USA. MASTER images were first corrected for the Bi-directional Reflectance Distribution Function (BRDF) effect to remove cross-track variation in reflectance amplitude. Two spectral indexes, the Normalized Difference Infrared Index (NDII) and the Normalized Difference Vegetation Index (NDVI), were derived from corrected morning and afternoon MASTER imagery and related to the field-measured CWC. At the ground level, a significant decrease (~9%) in CWC occurred from morning to afternoon ($p<0.0001$). The field-measured CWC was positively correlated with MASTER-derived NDII and NDVI for both morning (NDII: $r^2=0.67$, NDVI: $r^2=0.56$, $p<0.0001$) and afternoon (NDII: $r^2=0.42$, NDVI: $r^2=0.39$, $p<0.001$) data. The diurnal change in CWC also led to a statistically significant spectral change that was observed as a 4% decline in NDII ($p<0.005$) or 2% decline in NDVI ($p<0.0005$). Our results show that the diurnal variation in CWC can be detected for the irrigated orchards using simple spectral indexes derived from MASTER data, with higher sensitivity for NDII than for NDVI as expected. The results also demonstrate the potential for remote sensing to improve crop management and better understand plant physiological changes at field to regional scales.

1. Introduction

Mapping vegetation water status with remote sensing provides useful information to monitor plant drought stress (Peñuelas et al., 1993), assess fire risk (Chuvieco et al., 2002), manage irrigation of agricultural crops (Ben-Gal et al., 2009), and improve our understanding of the vegetation—climate relationship (Trombetti et al., 2008). One of the biophysical variables best related to optical remote sensing is vegetation canopy water content (CWC), which is the total amount of water accumulated in leaves per unit area (Cheng et al., 2008; Trombetti et al., 2008). Remotely sensed reflectance has been used to estimate CWC for different vegetation types such as chaparral shrubs (Serrano et al., 2000; Ustin et al., 1998), agricultural crops (Yilmaz et al., 2008b), broad-leaf trees (Colombo et al., 2008), and a mix of natural vegetation types (Ceccato et al., 2002).

Recently, Trombetti et al. (2008) produced a time series of CWC maps for the continental USA on a monthly basis using Moderate Resolution Imaging Spectrometer (MODIS) data from the Terra satellite, which showed good agreement with meteorological information across vegetation types. These time-series CWC data were useful for evaluation of seasonal variation in vegetation water status, but they were not meant to investigate CWC changes over shorter time periods, such as diurnal cycles. This diurnal CWC variation provides valuable information about the partitioning of surface energy and carbon exchange between vegetation and atmosphere, which increases our understanding of whether vegetation activities such as photosynthesis and evapotranspiration peak in the morning or afternoon (Wilson et al., 2003). Over the last decade, global networks such as FLUXNET around the globe have provided extensive diurnal micrometeorological data for the study of carbon, water, and energy cycles (Friend et al., 2007; Law et al., 2002; Wilson et al., 2002). The goal is to integrate station-based data with high temporal resolution satellite measurements in ecosystem models to resolve the daily cycles of carbon and water vapor exchanges. For example, Houborg and Soegaard (2004) derived land surface and atmospheric products from morning overpasses of MODIS and afternoon overpasses of the Advanced Very High Resolution Radiometer (AVHRR) and coupled them with an ecosystem model to compute diurnal ecosystem CO_2 and water vapor fluxes for an agricultural region. Airborne instruments provide the possibility to test new approaches and validate satellite retrieval algorithms since they can be flown under controlled conditions

* Corresponding author. Tel.: +1 530 752 5092; fax: +1 530 752 5262.
E-mail address: qtcheng@ucdavis.edu (T. Cheng).

0034-4257/$ – see front matter © 2013 Elsevier Inc. All rights reserved.
http://dx.doi.org/10.1016/j.rse.2012.12.024

(e.g., acquisition time, illumination geometry, and platform altitude) to detect diurnal changes in plant physiological status over experimental field sites (Sepulcre-Canto et al., 2006; Suárez et al., 2008).

MASTER, the MODIS/ASTER airborne simulator, generates image data with the spectral resolution acquired from MODIS and the Advanced Spaceborne Thermal Emission and Reflectance Radiometer (ASTER) and supports algorithm validation for the two spaceborne instruments (Hook et al., 2001). It can be mounted on various platforms to acquire imagery of different spatial resolutions and can be combined with other sensors such as the Airborne Visible/Infrared Imaging Spectrometer (AVIRIS) (Dennison & Matheson, 2011). Within the last decade, MASTER data have been successfully used for land cover classification that involves discrimination between vegetation types (Li & Moon, 2004; Mollot et al., 2007), among other applications. Although MODIS and Landsat 5 Thematic Mapper (TM) spectral bands have been investigated for estimating CWC (Cheng et al., 2008; Yilmaz et al., 2008b), similar studies using MASTER images have not been done, nor has anyone demonstrated detection of diurnal CWC changes with MASTER data.

The estimation of CWC from remotely sensed data generally relies on the leaf water absorption of radiation centered at 1240 nm, 1450 nm, and 1940 nm in the near infrared (NIR, 700 − 1350 nm) and shortwave infrared (SWIR, 1400 − 2500 nm) regions. Along with water-sensitive bands, a reference band in a NIR region (700 − 900 nm) can be used to construct spectral indexes that reduce the effect of variation in leaf internal structure, dry matter content and illumination variability (Ceccato et al., 2001). Common broadband spectral indexes developed for foliar water content retrievals include the Normalized Difference Infrared Index (NDII) (Hardisky et al., 1983) and the Normalized Difference Water Index (NDWI) (Gao, 1996). Recent studies, using data collected from the Soil Moisture Experiment (SMEX) field campaigns, have demonstrated the usefulness of NDII and NDWI for the estimation of CWC and total vegetation water content from satellite imagery (Chen et al., 2005; Cheng et al., 2008; Jackson et al., 2004; Yilmaz et al., 2008a, 2008b). Some of them have also reported water content estimations using the traditional Normalized Difference Vegetation Index (NDVI), for which a long-term record is available from satellite instruments, such as AVHRR and MODIS (Huete et al., 2002; Tucker et al., 2005). Although this canopy greenness based index tends to correlate with vegetation water content, it may not always be a good indicator of canopy water status as it is not directly related to canopy water absorption (Ceccato et al., 2001; Chen et al., 2005; Jackson et al., 2004).

To the best of our knowledge, no studies have been able to attribute diurnal changes in remotely sensed reflectance to diurnal dynamics of plant physiological properties. A major obstacle to this measurement is the impact of diurnal changes in the sun-target-sensor geometry on reflectance, which is termed the bi-directional reflectance distribution function (BRDF) effect (Meggio et al., 2008; Suárez et al., 2009). For example, Vanderbilt et al. (1991) could not conclusively attribute diurnal reflectance changes of two walnut canopies to changes in plant water status, primarily due to the BRDF effect. Suárez et al. (2008) related diurnal airborne observations of the Photochemical Reflectance Index (PRI) to several plant physiological indicators for water stress detection over an olive orchard. However, the contribution of BRDF remained mixed with that of water stress in the diurnal PRI changes. In turn, Hilker et al. (2008) adjusted their analysis for the BRDF effect and found that the strength of the observed relationship between tower-based measurements of photosynthetic efficiency and corrected canopy PRI over a conifer forest improved markedly (the r^2 increased from 0.37 to 0.82). The PRI was not originally designed to detect plant water status but to measure sun-mediated structural changes in xanthophyll cycle pigments in the visible spectrum, unaffected by water. Furthermore, those studies testing water–PRI relationships have been restricted either to a small part within an orchard measured in nadir positions or to a tower footprint area. Thus, it remains unclear whether it is feasible to detect water-induced diurnal spectral signals in nadir and off-nadir airborne data from canopies over larger geographic areas, such as orchards of 10s of km^2 with variable tree density, age, and species composition.

The objective of this study was to evaluate the potential of using MASTER data to detect diurnal CWC variation over agricultural crops for a better understanding of plant water status dynamics and crop water management. To detect subtle physiologically induced diurnal spectral differences, we designed an experiment that covered several pistachio and almond orchards of regularly spaced trees with homogeneous canopies. Field measurements of CWC were collected twice during the course of a day to support morning and afternoon acquisitions of MASTER imagery. Spectral indexes derived from MASTER data were used to relate observed spectral changes to changes in CWC. This study establishes the basis for detecting diurnal CWC variation over broad geographic areas using morning and afternoon MODIS overpasses.

2. Materials and methods

2.1. Study site

The study site is a flat agricultural area located in western Kern County, CA (35°29′45″ N, 119°40′2.6″ W) and comprises 10 km^2 of irrigated pistachio and almond tree orchards near Lost Hills, California (Fig. 1). Three blocks of pistachios and eight of almonds (approximately 800 × 800 m each) were chosen to represent combinations of age, variety, and irrigation schedule (Table 1). The rows are oriented in the north − south direction. Six blocks (labeled as BE_002, BE_004, BE_005, BE_006, BE_007, and BE_008 in Fig. 2) are divided into three approximately equal-sized irrigation sets (west, middle, and east) while blocks BE_009 and BE_011 are divided into four irrigation sets and BE_010 into five sets. While trees in blocks BE_010 and BE_011 are diagonally spaced and exhibit different canopy densities every few rows, trees in other blocks are parallel spaced and form more homogeneous canopies. Scheduled irrigation is managed by Paramount Farming Company (Bakersfield, CA) and applied to all sets within each block sequentially from west to east, except for the two pistachio blocks BE_001 and BE_003 that are irrigated as a whole.

2.2. Sampling design

Due to practical constraints, our data collection was limited to two plots in the same tree row per irrigation set in each of the eleven blocks. Each plot represented a 3 × 3 tree area, which is approximately 324 m^2. The plot locations were selected to span a wide range of vegetation density, structure conditions, and vegetation water content based on NDII and NDVI images from MASTER data acquired in 2009 under NASA's Student Airborne Research Program (SARP). To reduce potential noise in plot spectral signatures due to image misregistration and errors in plot geolocation, each plot was chosen as the central part of a larger spatially homogeneous area. We located these tree plots using 1-meter resolution USGS Digital Orthophoto Quarter-Quadrangle (DOQQ) aerial imagery and linked them to the locations in MASTER imagery.

2.3. Field data collection

Collecting timely field data is important to detecting and validating diurnal CWC differences. Ideally, ground measurements should be acquired synchronously with the flight. In our experiment this ideal situation was unattainable due to practical limitations in the field work resources and field crew availability. Therefore, we conducted all leaf sampling within a three-day period: one day before, on the flight day, and one day after the flight. The weather conditions were stable during such a short sampling period (see Table 2). Furthermore, our sampling plan accounted for the irrigation schedule in these orchards. In particular, plots irrigated the day before the flight were sampled only on the

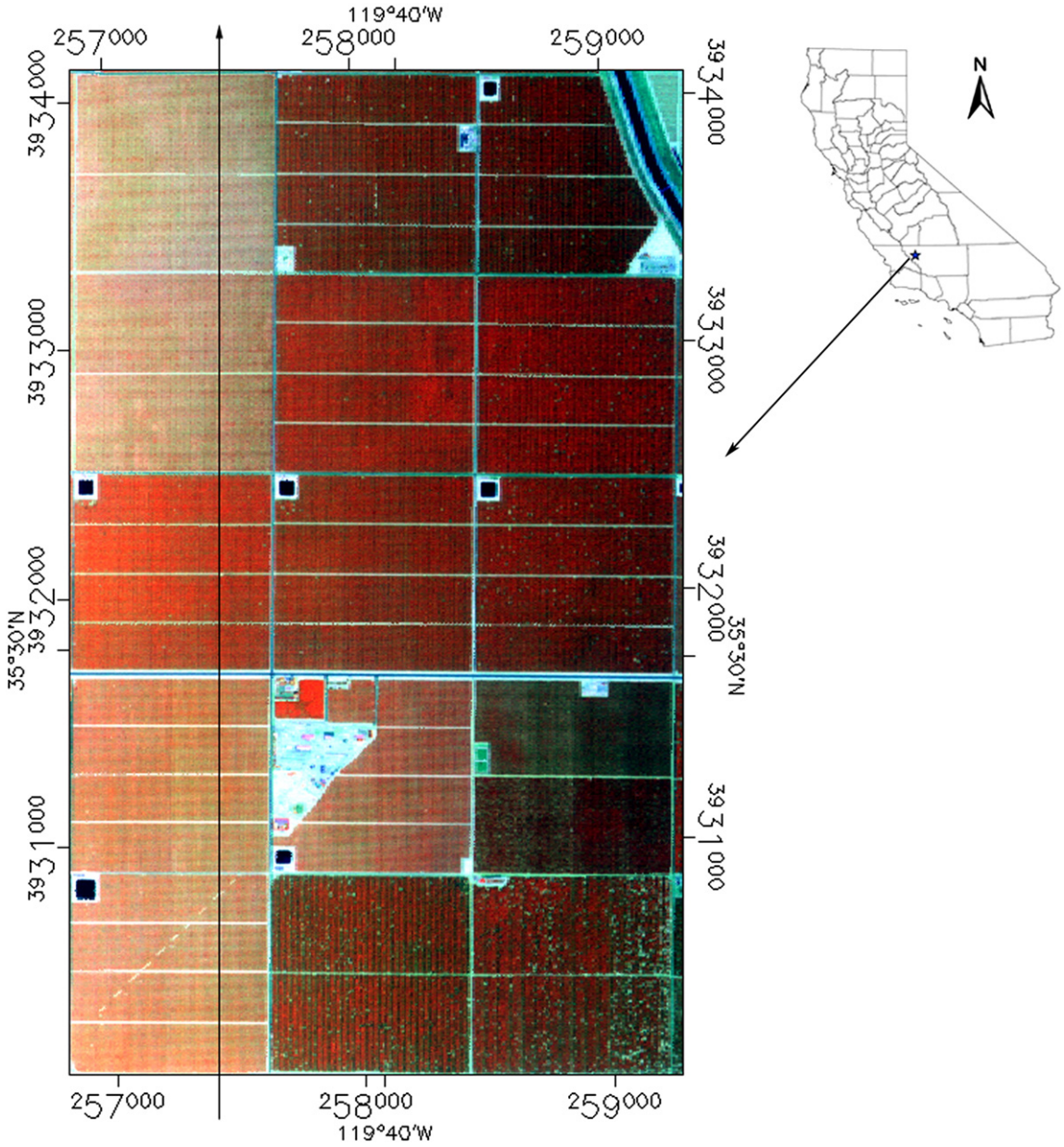

Fig. 1. Study site near Lost Hills, California, USA as seen from a MASTER image acquired in the morning of June 29, 2010. Band combinations for this false color composite are MASTER bands 9 (872 nm), 13 (1667 nm), and 5 (658 nm). The black line with an arrow indicates the path and direction of MASTER instrument for both morning and afternoon flight overpasses. Squares exhibiting relatively homogeneous vegetation cover are 800×800 m orchard blocks.

flight day, and plots irrigated on the flight day were not sampled on the following day, so that the water uptake by the time of MASTER overpass would be minimal. Leaf sampling occurred from 0900 h to 1100 h Pacific Standard Time (PST) for morning measurements and 1300 h to 1500 h PST for afternoon measurements. Twenty leaves were collected with tree pruners (extendable to 4.3 m) from each of nine trees in the plot: ten leaves on the sunny side and ten leaves on the shady side of the outer canopy that would be visible from above. All leaf samples from the nine trees were sealed in plastic zip-lock bags and kept in coolers immediately after detaching from branches, avoiding direct contact with the ice until fresh weight and leaf surface area measurements could be made at a local laboratory provided by Paramount Farming Company. The fresh weight (FW) of leaf samples was determined using an Acculab VIC-303 Vicon Digital Balance (0.001 g). Leaf area (A) was automatically calculated with up to 5% uncertainty from scanned images of Epson Perfection V30 color scanners using Matlab (MathWorks, Massachusetts, USA). This accuracy was determined by scanning ten times a 50 cm^2 calibration disc placed at different positions on a scanner. Dry weight (DW) was determined after all samples were dried in an oven at 60 °C for 48 h (Chuvieco et al., 2002; Davidson et al., 2006). The leaf water content was expressed as the equivalent water thickness (EWT, g/cm^2) as:

$$EWT = \frac{FW - DW}{A}. \quad (1)$$

To scale the water content from leaf to canopy level, the leaf area index (LAI, m^2/m^2) over each plot was determined using digital hemispherical photography. Twelve hemispherical photographs per plot were acquired midway between trees under diffuse sunlight conditions around sunset or sunrise, with six photos in the aisles and six in the tree rows. The LAI was assumed constant during the seven day period needed for taking all photos. All photographs were processed with HemiView (Delta-T Devices Ltd., Cambridge, UK) to calculate

Table 1
Block characteristics of the orchards in the study area.

Block name	Year planted	Species	Variety	Irrigation system	Row spacing (m)	Tree height (m)
BE.001	2000	Pistachio (*Pisctachio vera* L.)	Kerman	Drip	5.8	1.5–2.5
BE.002	2000	Almond (*Prunus dulcis*)	Butte, padre, ruby	Fan jet	7.5	4.0–7.0
BE.003	2000	Pistachio (*Pisctachio vera* L.)	Kerman	Drip	5.8	2.0–3.0
BE.004	1999	Almond (*Prunus dulcis*)	Monterey, nonpareil	Drip and fan jet	7.5	2.5–7.0
BE.005	1999	Almond (*Prunus dulcis*)	Monterey, nonpareil	Fan jet	7.5	4.0–8.0
BE.006	1999	Almond (*Prunus dulcis*)	Monterey, nonpareil	Fan jet	7.5	3.0–6.5
BE.007	2000	Almond (*Prunus dulcis*)	Monterey, nonpareil, wood colony	Fan jet	7.5	3.5–7.0
BE.008	2006	Almond (*Prunus dulcis*)	Monterey, nonpareil	Fan jet	7.5	3.0–4.5
BE.009	1985	Pistachio (*Pisctachio vera* L.)	Kerman	Fan jet	7.5	2.0–5.0
BE.010	1988	Almond (*Prunus dulcis*)	Carmel, price, nonpareil, padre	Fan jet	5.8, 6.5	4.5–8.0
BE.011	1994	Almond (*Prunus dulcis*)	Carmel, price, nonpareil, padre	Fan jet	5.8, 6.5	4.0–8.0

LAI values. The LAI for a plot was determined as the average of twelve LAI values calculated from each of the photographs. The CWC (g/cm^2) was calculated as:

$$CWC = EWT \times LAI. \quad (2)$$

EWT was measured in the morning and afternoon to examine the diurnal differences. Due to the long process of CWC measurements spanning from leaf sampling to leaf scanning, leaf weighing and fisheye photography and time sensitivity of diurnal signals, we were able to acquire complete CWC data for 28 plots out of the 66 designed plots (33 irrigation sets × 2 plots per set) in the strictly specified time window. The acquired plots represented both pistachio and almond with a range in EWT from 0.010 to 0.023 g/cm^2 (mean ± s.d. = 0.017 ± 0.0027 g/cm^2 for morning and 0.015 ± 0.0029 g/cm^2 for afternoon). The range in LAI was 0.71 to 1.90 m^2/m^2 (mean ± s.d. = 1.36 ± 0.34 g/cm^2) (Fig. 3).

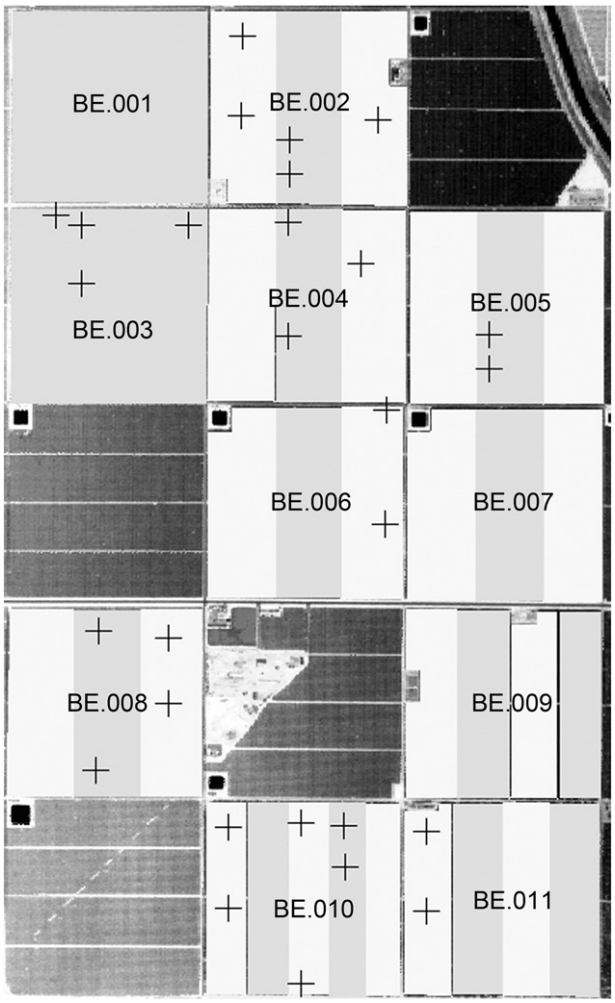

Fig. 2. Orchard square blocks (labeled as BE.001, BE.002, …, BE.011), 28 field plots ("+" symbols) with valid ground data and 33 irrigation sets (white and gray polygons) overlaid on a MASTER image of the study area. Note that some irrigation sets have no plots with valid ground data but they are still included in this figure because showing all irrigation sets will make it easier to compare this study to other relevant studies that may have valid data for different plots.

2.4. Remotely sensed data

2.4.1. Image acquisition

The MASTER instrument was flown on a NASA DC-8 aircraft at an altitude of 4000 m on June 29, 2010 from south to north (Fig. 1), and passed over the study site twice under clear skies to acquire morning (1050 h PST) and afternoon (1305 h PST) imagery. The acquisition times, approximately 1 h before and 1 h after the solar noon (1200 h PST), resulted in solar zenith angles (SZAs) of 19.8° and 18.5°, respectively. These acquisitions had approximately symmetric solar geometry around solar noon and therefore minimized the difference in amounts of shadow within the row-structured canopies and the effect of diurnal variation in SZA on canopy reflectance. The average air temperature on the flight day was 27.3 °C (Table 2), which is 3.6 °C higher than the 10-year average for that day. The MASTER collected MODIS-like and ASTER-like data in 50 channels but only the 25 reflective bands with wavelength ranges from 0.4 to 2.5 μm were used in this study. The sensor records 716 pixels per scan line in cross-track direction with an instantaneous field of view of 2.5 mrad. The field of view (FOV) is 85.92° and the maximum view zenith angle (VZA) is ±42.50°, with negative angles representing scanning on the west side and positive angles on the east side of the flight line.

2.4.2. Image preprocessing

The MASTER radiance data distributed in L1B level format were atmospherically corrected to retrieve apparent surface reflectance using FLAASH (Fast Line-of-sight Atmospheric Analysis of Spectral Hypercubes) that is a MODTRAN-4-based correction algorithm available in the ENVI software package (Exelis Visual Information Solutions, Boulder, CO) (Matthew et al., 2003). The atmospheric correction

Table 2
Weather conditions for the field sampling period. Data are acquired by the closest California Irrigation Management Information System (CIMIS) station (CIMIS #146: http://www.cimis.water.ca.gov/cimis/welcome.jsp) that is 800 m away in the west of block BE.003.

Date	Average air temperature (°C)	Average wind speed (m/s)	Average relative humidity (%)	Precipitation (mm)
6-28-2010	29.1	1.6	48	0
6-29-2010	27.3	1.5	48	0
6-30-2010	26	1.5	43	0

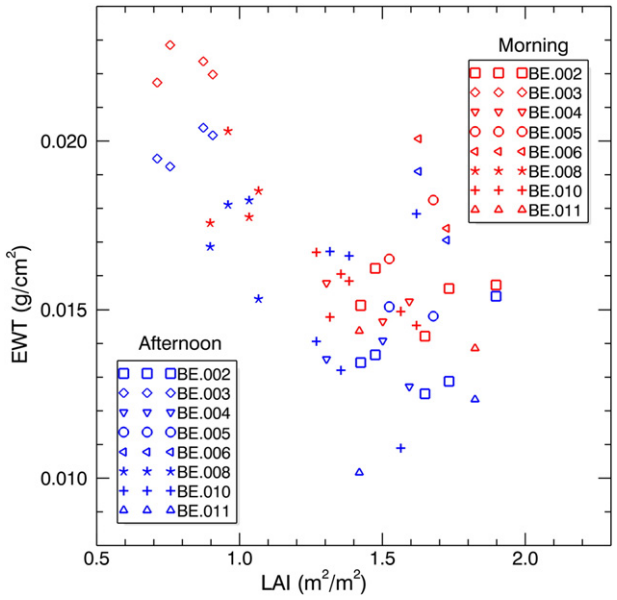

Fig. 3. A scatter plot of leaf area index (LAI) versus equivalent water thickness (EWT) collected from the study site. Morning (red symbols) and afternoon (blue symbols) EWT measurements were available for each of the 28 field plots. (For interpretation of the references to color in this figure legend, the reader is referred to the web version of this article.)

for both images was based on a mid-latitude summer atmospheric model and rural aerosol model. The retrieved reflectance images were georeferenced using input geometry information distributed with the raw data, which generated a spatial resolution of 5.6 m for the morning image and 5.8 m for the afternoon image. The afternoon image was resampled to the spatial resolution of the morning image (5.8 m) by pixel aggregation, which averages all the 5.8-m-pixel values that contribute to the output 5.6-m-pixel. The alignment errors between two images were within one pixel. Both morning and afternoon MASTER images were registered against the 1-meter resolution DOQQ image using a pure translation estimated with manually chosen corresponding points and nearest neighbor interpolation. The registration accuracy achieved this way was sufficient for our hypothesis tests to yield statistically significant results presented in Section 3.1.

Due to the wide scan angle of MASTER and the diurnal variation in solar position, both morning and afternoon images had exhibited obvious cross-track brightness gradients (Fig. 4). The VZA varied from −9° to 24° as the MASTER instrument scanned each line in the cross-track direction. The morning image appears brighter on the west side and darker on the east side in a false color composite (Fig. 1) and the afternoon image shows the opposite trend (image not shown), which demonstrates the BRDF effect (Beisl, 2001; Sandmeier & Itten, 1999). This effect increases as VZA increases until it reaches the hot spot area (i.e., VZA = SZA), preventing an effective comparison of morning observations to afternoon observations of the same targets at off-nadir positions.

To minimize the spectral contribution from the BRDF effect, we followed a class-wise empirical correction approach proposed by Kennedy et al. (1997). This method models the VZA-dependent bidirectional reflectance factor (BRF) (i.e., cross-track brightness gradient) per land surface type and then normalizes off-nadir BRFs to the nadir view. Instead of the iterative optimization classification in Kennedy et al (1997), a spectral-index-based method was used to classify the images into broad 'BRDF classes'. By applying NDVI thresholds to the uncorrected morning image, the study area was classified into three canopy structural types: non-vegetation, sparse vegetation, and dense vegetation. Furthermore, pixel-members from the same column for each class were averaged to derive BRFs as polynomial functions of their common VZA. For each class, a third-order polynomial model of the BRF was found to account for the hot spot effect better than second-order polynomials that were used in the cases of no hot spot effect (all VZAs were less than the SZA) (Kennedy et al., 1997; Schiefer et al., 2006). The BRFs for the soil class were not modeled. The brightness gradients were removed by dividing all reflectance values by a class-specific multiplicative compensation factor that is defined by Kennedy et al. (1997) as a ratio of modeled BRFs for all VZAs to the BRF at nadir positions (Schiefer et al., 2006). Fig. 5 demonstrates that our BRDF correction has markedly reduced the large diurnal cross-track variation in morning and afternoon reflectance data, which was obvious in Fig. 4.

The spectral signatures of each plot were extracted by averaging the BRDF-corrected image spectra in a 3×3 pixel window centered at the plot center. Using the mean spectra is known to reduce noise in comparing field-based and image-derived quantities (see also Section 2.2). These signatures were used to calculate spectral index values for further statistical analyses. Since the water band for another commonly used water index NDWI is unavailable for MASTER, this study used the NDII water index and included the widely used greenness index NDVI as a reference. The MASTER-derived NDII is calculated as:

$$\mathrm{NDII} = \frac{R_{nir} - R_{swir}}{R_{nir} + R_{swir}} = \frac{\text{band 9} - \text{band 13}}{\text{band 9} + \text{band 13}} \quad (3)$$

and the NDVI is calculated as:

$$\mathrm{NDVI} = \frac{R_{nir} - R_{red}}{R_{nir} + R_{red}} = \frac{\text{band 9} - \text{band 5}}{\text{band 9} + \text{band 5}}. \quad (4)$$

The center wavelengths for MASTER bands 5, 9, and 13 are 658 nm, 872 nm, and 1667 nm, respectively. The two NDII bands in MASTER are also available in MODIS on board the Terra and Aqua satellites and have already been applied to large scale monitoring of drought stress (Fensholt & Sandholt, 2003).

2.4.3. Statistical tests

A paired Student's *t*-test in R version 2.12.0 (R Development Core Team, 2010) was used to statistically test the hypothesis that the difference between mean morning and afternoon CWC values is positive against the null-hypothesis of no difference. This test was applied for

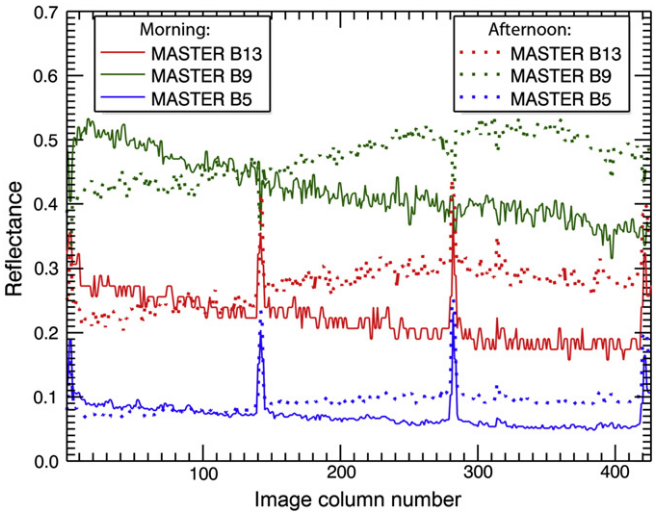

Fig. 4. Horizontal profiles of reflectance extracted from uncorrected morning and afternoon MASTER images for a cross-track transect passing through blocks BE_006 and BE_007 as shown in Fig. 2. Red, green and blue lines represent cross-track variation in reflectance of uncorrected morning (solid lines) and afternoon (dashed lines) images for MASTER bands 13, 9 and 5, respectively. (For interpretation of the references to color in this figure legend, the reader is referred to the web version of this article.)

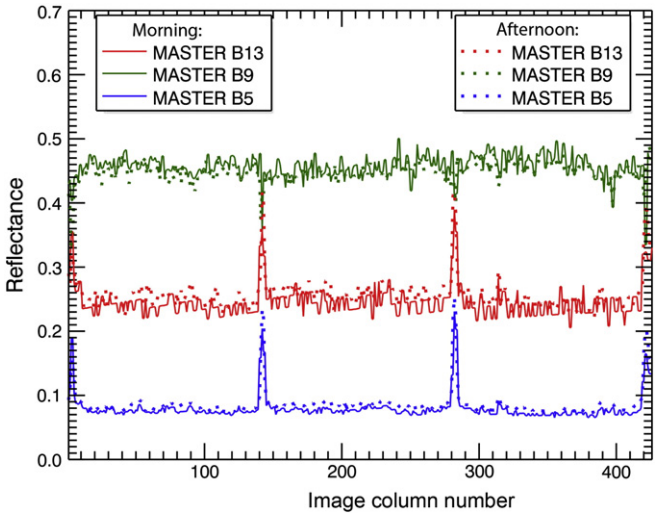

Fig. 5. Horizontal profiles of reflectance extracted from corrected morning and afternoon images for the same transect as shown for Fig. 4. Red, green and blue lines represent cross-track variation in reflectance of corrected morning (solid lines) and afternoon (dashed lines) images for MASTER bands 13, 9 and 5, respectively. (For interpretation of the references to color in this figure legend, the reader is referred to the web version of this article.)

three types of CWC: the field-measured CWC and the CWC estimated by the MASTER-derived NDVI and NDII. Since the results of a paired *t*-test may be affected by substantial deviation of the underlying sample distribution from a normal distribution, we also applied a permutation test (Moore & McCabe, 2006). We ran the permutation test in R and used 9999 permutations, thus allowing an approximation of the *p*-value with accuracy up to 10^{-4}. The one-sided test *p*-value was conventionally approximated as the proportion of permutations in which the diurnal difference in mean CWC was not positive, where the term "diurnal difference" means morning CWC minus afternoon CWC. The statistical significance of correlations between CWC and MASTER-derived NDVI and NDII was evaluated using bootstrap confidence intervals. A correlation was considered significant if a 95% confidence interval of the correlation coefficient did not include 0.0.

3. Results

3.1. Relationship between field-measured CWC and MASTER-derived vegetation indexes

Fig. 6A shows a histogram of the CWC difference values measured for the 28 field plots. A paired *t*-test supports that the afternoon CWC (0.21 ± 0.047 kg/m^2 for mean ± s.d.) was significantly lower than the morning CWC (0.23 ± 0.044 kg/m^2) ($p<0.0001$) and the permutation test confirmed the significance ($p=0.0001$).

The MASTER-derived NDII and NDVI for morning, afternoon, and combined times were found significantly correlated with the field-measured CWC (Fig. 7). Overall, the correlation of NDII to CWC was stronger than NDVI to CWC, as expected based on differences in sensitivity to water. For morning data, NDII correlated to CWC with an r^2 of 0.67 ($p<0.0001$) and NDVI correlated to CWC with an r^2 of 0.56 ($p<0.0001$). The correlations were weaker for afternoon data with an r^2 of 0.42 ($p<0.0005$) for NDII and 0.39 ($p<0.001$) for NDVI. The bootstrap confidence interval analysis also indicated all correlations between MASTER-derived NDII and NDVI and field-measured CWC were statistically significant.

An analysis of the covariance (ANCOVA) shows the regression models, derived from the morning data and the afternoon data separately, had no differences in slopes (NDII: $p=0.56$, NDVI: $p=0.88$) and only marginal differences in intercepts (NDII: $p=0.07$, NDVI: $p=0.08$). This allowed us to generate a single CWC~NDII or CWC~NDVI model by combining morning data and afternoon data (Fig. 7, NDII: $r^2=0.53$, $p<0.0001$; NDVI: $r^2=0.47$, $p<0.0001$). Using the regression models derived from combined data, the ranges of estimated diurnal differences were narrower than that of field-measured diurnal differences. However, for most plots the estimated diurnal differences were still positive (Fig. 6B and C). The estimated afternoon CWC was significantly lower than the estimated morning CWC for both NDII ($p<0.005$ for both tests) and NDVI ($p<0.0005$ for both tests). The diurnal water loss in the canopies for the field plots was measured as ~9% (morning vs afternoon: 0.23 kg/m^2 vs 0.21 kg/m^2) of respective CWC values and resulted in detectable spectral changes as 4% in NDII (morning mean NDII $=0.24 \pm 0.069$; afternoon mean NDII $=0.23 \pm 0.069$) and 2% for NDVI (morning mean NDVI $=0.64 \pm 0.082$; afternoon mean NDVI $=0.63 \pm 0.077$).

3.2. Mapping CWC using spectral indexes

After applying the NDII–CWC relationship obtained for combined data to respective morning and afternoon images, the spatially explicit CWC estimates are displayed as maps in Fig. 8A and B, and their difference is displayed in Fig. 8C. The two CWC maps show similar spatial patterns across irrigation sets within most blocks (BE_002, BE_004, BE_006, BE_009, BE_010, and BE_011). On the difference map (Fig. 8C), positive differences represent declines in CWC during the course of a day and are mostly seen for blocks with dense canopies (BE_002, BE_004, BE_005, BE_006, BE_007, and on the eastern half of BE_009). This is supported by the irrigation-set-level diurnal differences in CWC (Table 3), which are generally greater for these blocks than for other blocks.

Fig. 9 shows morning CWC, afternoon CWC, and their difference derived by applying the NDVI–CWC relationship to respective NDVI images. The three images show similar spatial patterns to Fig. 8 but have less contrast in either CWC or CWC difference. The CWC estimates derived from NDVI images are generally lower than those from NDII. The CWC differences estimated by NDVI were mostly higher than those estimated by NDII for blocks with sparse canopies (BE_001, BE_003, and BE_008) and with a more irregular planting structure (BE_010 and BE_011) (Table 1).

At the irrigation-set level, the MASTER-derived CWC of most canopies decreased over the diurnal cycle, which is supported by significantly lower afternoon CWC values than morning CWC values estimated by either NDII or NDVI ($p<0.0001$ for the paired *t*-test and $p=0.0001$ for the permutation test). We did not stratify our analysis by irrigation set due to insufficient sampling.

4. Discussion

This study investigates diurnal variation in vegetation water status via CWC derived from remotely sensed data. The diurnal CWC variation was driven by changes in leaf EWT since there was little change in LAI during the sampling period. Leaf angle is an important factor in deriving canopy reflectance variation (Ollinger, 2011), but it was not likely to change substantially at image acquisition times while the canopies were exposed to similar solar radiation (Rosa & Forseth, 1996). The water status in trees changes over the course of a day as a result of water loss dynamics through transpiration (Breda et al., 2006; Simonneau et al., 1993). Irrigation did not change between the times of flight overpasses (1050 h PST and 1305 h PST) and the water uptake from soil to leaves was expected to approximate the atmospheric demand. Crop water use can be determined from measurements of evapotranspiration (ET) that include the loss of water from canopies through transpiration and evaporation from soil surfaces (Ham et al., 1990; Jung et al., 2010). In these well-irrigated orchards, water supply was sufficient to avoid potential yield loss. The fully developed canopies, especially those of higher density,

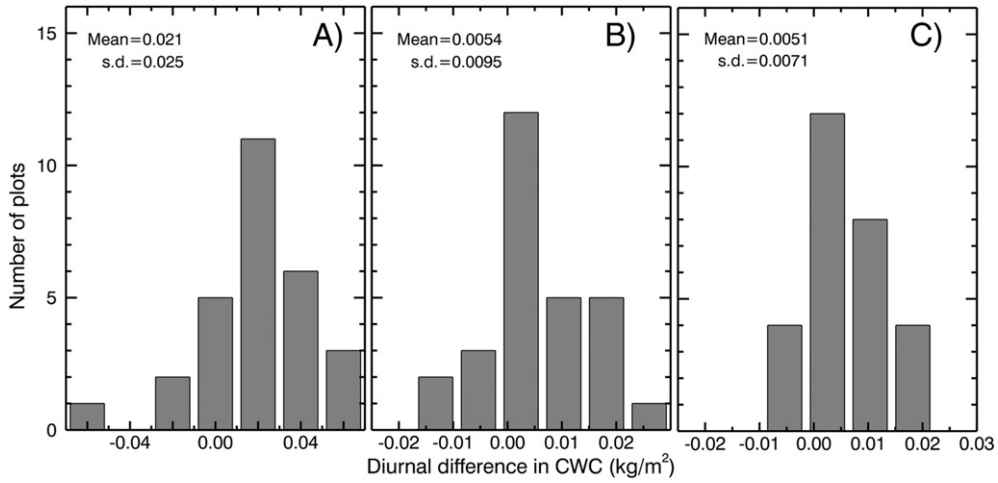

Fig. 6. Histograms of diurnal differences in CWC for the 28 field plots with reference to theoretical normal distributions (smooth lines). These differences between morning and afternoon CWC values are (A) measured in the field, (B) estimated by MASTER-derived NDII, and (C) estimated by MASTER-derived NDVI. Positive difference values indicate declines in diurnal CWC. Data in the histograms all passed the Shapiro–Francia normality test ($p>0.05$) as closely matched to normal distributions.

should be at high transpiration rate (1 h before and after mid-day) and it was more likely for transpiration to play an important role in ET changes than for soil evaporation (Sauer et al., 2007). The water decline in the afternoon as observed from ground and airborne data suggested that the orchards were not able to maintain a constant amount of canopy water. Therefore, canopy water loss during the time that elapsed between image acquisitions could be explained by an increase in ET from morning to afternoon. The incident solar radiation peaks at solar noon on a clear day, but ET that is driven by incident solar radiation and temperature lags behind and reaches its maximum in the mid-afternoon (Choudhury & Idso, 1985; Reicosky et al., 1982; Weber & Ustin, 1991; Wilson et al., 2003). This observation is consistent with the standard ET (ET_o) value recorded by the nearest CIMIS station (Fig. 10) as 0.73 mm/h at 1100 h PST with an air temperature of 31.6 °C and 0.81 mm/h at 1300 h PST with an air temperature of 34.2 °C (downloaded from http://www.cimis.water.ca.gov/cimis/data.jsp). For the 28 field plots, we observed significant diurnal differences in CWC both physiologically and spectrally. The diurnal spectral changes caused by a 9% change in CWC over the experimental site are sufficiently significant to be detected using airborne remotely sensed imagery. We also observed a similar behavior in the data from June 28 (9 field plots) and June 29 (15 field plots) separately, but the stratifying analysis by sampling day would have greatly decreased the variability in tree characteristics and therefore weakened our findings.

In general, remote detection of diurnal changes in CWC is challenging because the observed difference can be attributed to a number of confounding factors, such as variation in the solar position, physiological status, growth stage, atmospheric conditions, topography, shadowing, and imaging parameters. Furthermore, many studies have pointed out that remote sensing images must be corrected for any BRDF effect to meaningfully interpret the apparent temporal variation in vegetation indexes (Galvao et al., 2004, 2011; Los et al., 2005). This orchard study minimized a number of target geometry factors because of consistent growth stage of the trees and flat terrain. Also, the dual airborne flights conducted within a small time window (2 h) under clear-sky conditions minimized the variation in solar illumination intensity and atmospheric conditions. Our target signature was still found to originate from the spectral response to diurnal changes in physiological status although it was influenced by variations in VZA and SZA. We minimized these variations by scheduling the two flights so that the overpass times were symmetric about solar noon and choosing the North–South flight directions parallel to the row orientation, and conducting an empirical BRDF correction

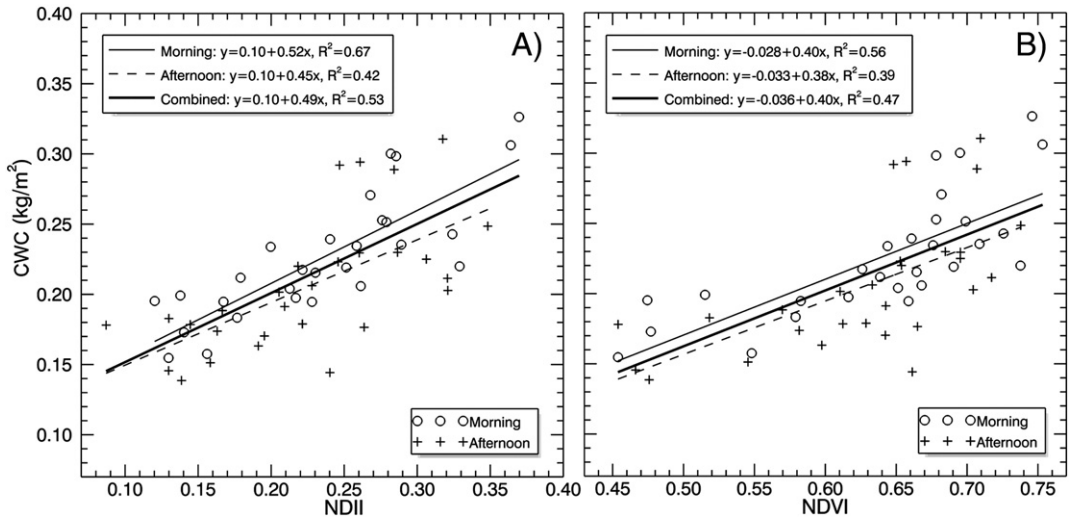

Fig. 7. Relationships between field-measured CWC and MASTER spectral indexes (A) NDII and (B) NDVI for the 28 field plots with valid ground data in the morning (circles) and afternoon (pluses).

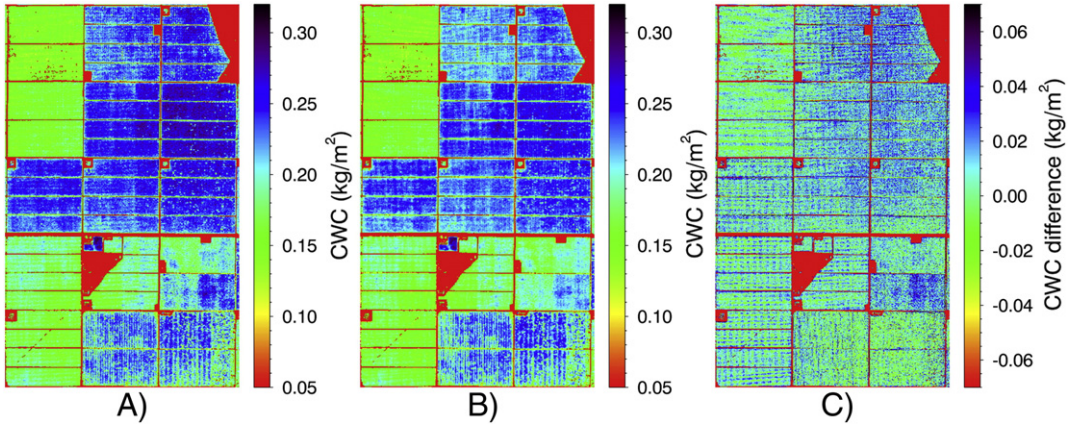

Fig. 8. CWC maps derived from MASTER NDII data. Images (A) and (B) represent CWC produced by applying the combined model in Fig. 7A to morning and afternoon NDII images, respectively. Greater values in scale bars represent wetter orchard canopies. Image (C) displays the pixel-wise difference between (A) and (B) and represents diurnal CWC variation, with positive values indicating declines in diurnal CWC. Non-vegetated areas are excluded from CWC analysis and always shown in red. (For interpretation of the references to color in this figure legend, the reader is referred to the web version of this article.)

of the diurnally acquired images for the BRDF effect. This flight design would not minimize the BRDF effect but made it easier to understand the effect and to run image post-processing. It also precluded the correction for the influence of diurnal solar illumination variability.

Although using normalized difference indexes, such as NDII and NDVI, to estimate CWC partially compensates for the diurnal differences in imaging conditions, it does not effectively remove the BRDF effect. For example, an earlier work by Cheng et al. (2011) shows that CWC maps derived from uncorrected NDII data exhibit cross-track brightness gradients due to the BRDF effect. They found this effect was weak in both morning and afternoon images but was amplified on the CWC difference map due to the opposite trends (Fig. 4) in the morning and afternoon images. After the BRDF correction described in Section 2.4.2, the morning reflectance data were comparable in magnitude to the afternoon reflectance data (Fig. 5) and the cross-track gradients disappeared (Figs. 8 and 9). Thus, the BRDF correction helped separate the water-induced spectral response from directional spectral variation. Despite the removal of cross-track brightness gradients, we did not observe an increase in r^2 for the CWC–NDII or CWC–NDVI relationship due to an insufficient number of samples at off-nadir positions (e.g. BE_007 and BE_009) for the evaluation (Fig. 2). Suárez et al. (2008) reported one of few airborne observations of diurnal vegetation dynamics in the literature and found that canopy PRI was sensitive to diurnal changes in such physiological indicators of water stress as stomatal conductance, stem water potential, steady-state fluorescence, and crown temperature. They determined three independent regression models without BRDF correction for PRI data acquired at 07:30, 09:30, and 12:30 GMT, but did not provide a universal model that fit the pooled PRI and physiological data. We compared their diurnal physiological data to canopy PRI from the three regression models, and suspect their systematic offset of PRI with time of day indicates a BRDF influence. This example illustrates the importance of BRDF correction in analyzing vegetation dynamics with diurnal remote sensing data.

The spectral indexes NDVI and NDII underestimated the ~9% field measured diurnal change in CWC by different amounts: the NDII showed a 4% change and the NDVI detected 2% change. Indeed, the CWC correlated more strongly to the water sensitive index NDII ($r^2 = 0.53$) than the greenness sensitive index NDVI ($r^2 = 0.47$). The NDII is directly related to the strength of water absorption in the SWIR region and is more sensitive to the contrast in water content between sparse canopies and dense canopies (Fig. 8). The weaker correlation of NDVI than water indexes with canopy water absorption was also found by Cheng et al. (2006) at agriculture and forest sites. The lower correlation for NDVI is consistent with the fact that the chlorophyll content represented by NDVI may not always be well related to canopy water content (Ceccato et al., 2001). Nevertheless, the NDVI–CWC scatter plot in Fig. 7B has more data points near the upper end of the regression line, which indicates lower sensitivity of NDVI to CWC changes for plots with NDVI higher than 0.65 although the LAI measurements for our study are generally low (LAI: 0.7 to 1.9). This saturation is also supported by the generally

Table 3
Summary of diurnal differences in MASTER-derived CWC using NDII and NDVI. Each value in the table is obtained by averaging the difference between morning and CWC and afternoon CWC over all pixels in the irrigation set area. The first two columns are absolute CWC differences and the last two columns are CWC differences relative to morning CWC values.

Irrigation SET	CWC difference by NDII (kg/m^2)	CWC difference by NDVI (kg/m^2)	Ratio of CWC difference to morning CWC by NDII (%)	Ratio of CWC difference to morning CWC by NDVI (%)
BE.001	0.0012	0.0013	0.48	0.81
BE.002.SET.1	0.0076	0.0074	3.05	2.99
BE.002.SET.2	0.0159	0.0128	6.56	5.17
BE.002.SET.3	0.0183	0.0138	7.37	5.49
BE.003	0.0008	0.0012	0.17	0.59
BE.004.SET.1	0.0086	0.0077	3.33	3.06
BE.004.SET.2	0.0125	0.0116	4.94	4.63
BE.004.SET.3	0.0118	0.0121	4.10	4.45
BE.005.SET.1	0.0157	0.0104	5.34	3.48
BE.005.SET.2	0.0121	0.0088	4.05	3.09
BE.005.SET.3	0.0132	0.0086	4.71	3.14
BE.006.SET.1	0.0091	0.0090	3.81	3.72
BE.006.SET.2	0.0083	0.0097	3.38	4.08
BE.006.SET.3	0.0138	0.0125	5.46	5.08
BE.007.SET.1	0.0107	0.0097	3.95	3.66
BE.007.SET.2	0.0091	0.0078	3.22	2.81
BE.007.SET.3	0.0062	0.0059	2.12	2.19
BE.008.SET.1	0.0047	0.0062	2.47	3.32
BE.008.SET.2	0.0048	0.0050	2.46	2.58
BE.008.SET.3	0.0059	0.0062	3.17	3.24
BE.009.SET.1	0.0109	0.0114	5.21	5.48
BE.009.SET.2	0.0090	0.0105	4.04	4.84
BE.009.SET.3	0.0163	0.0127	6.74	5.43
BE.009.SET.4	0.0121	0.0113	4.90	4.89
BE.010.SET.1	0.0060	0.0028	2.46	0.97
BE.010.SET.2	0.0031	0.0018	0.87	0.59
BE.010.SET.3	0.0008	0.0009	−0.21	0.19
BE.010.SET.4	−0.0001	0.0016	−0.78	0.46
BE.010.SET.5	−0.0017	0.0013	−1.37	0.42
BE.011.SET.1	−0.0009	0.0024	−0.91	0.94
BE.011.SET.2	−0.0022	0.0028	−1.65	1.05
BE.011.SET.3	−0.0001	0.0040	−0.50	1.64
BE.011.SET.4	0.0025	0.0059	0.57	2.59

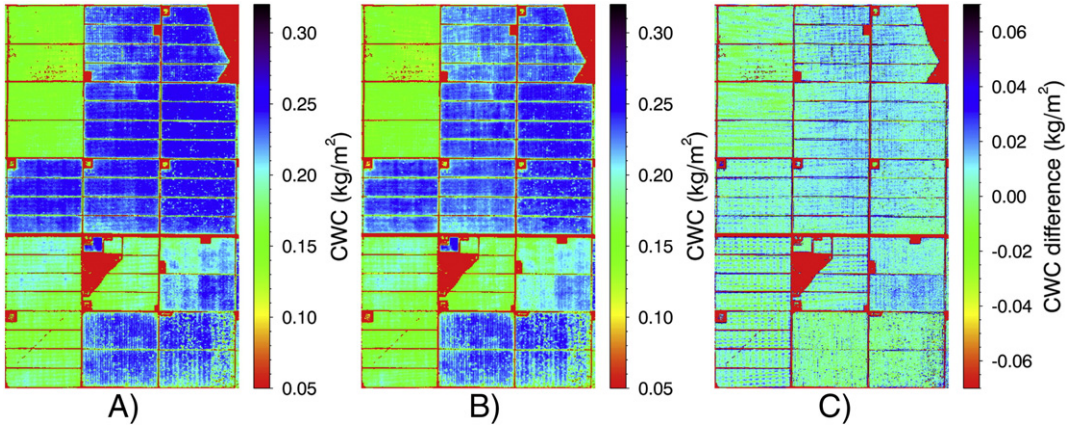

Fig. 9. CWC maps derived from MASTER NDVI data. Images (A) and (B) represent CWC produced by applying the combined model in Fig. 6B to morning and afternoon NDVI images, respectively. Greater values in scale bars in (A) and (B) represent wetter orchard canopies. Image (C) displays the pixel-wise difference between (A) and (B) and represents diurnal CWC variation, with positive values indicating declines in diurnal CWC. Non-vegetated areas were excluded from the CWC analysis and always shown in red. (For interpretation of the references to color in this figure legend, the reader is referred to the web version of this article.)

lower magnitude in the NDVI-derived CWC maps for dense canopies (Fig. 9).

The orchards were mostly irrigated from west to east within each block using block-specific schedules. We did not find a significant relationship between the number of days since irrigation and CWC or CWC differences (data not shown). Only a few blocks (BE_002, BE_004, and BE_006), indicated a systematic CWC gradient from west to east due to the difference in the number of days since irrigation. Our data were collected in the middle of growing season when the crops were being well irrigated to avoid yield loss and water supply was sufficient, which could explain why the water status was less affected by the irrigation schedule. In addition, blocks BE_010 and BE_011 on the CWC maps (Fig. 8A and B) showed stripe patterns in a north–south direction that were due to different planting strategies across tree rows.

For some pixels, their soil background was visible to the sensor and therefore the diurnal changes in soil moisture might have contributed to the remotely sensed CWC change. To test the effect of variation in soil moisture on NDII and NDVI, we ran the commonly used radiative transfer model PROSAIL (Baret et al., 1992; Jacquemoud et al., 2009), which couples the leaf optical properties model PROSPECT (Féret et al., 2008; Jacquemoud & Baret, 1990) and the canopy reflectance model SAIL (Verhoef, 1984; Verhoef et al., 2007). Fig. 11A shows a series of soil reflectance spectra with variable moisture content, which is represented in PROSAIL by a soil wetness coefficient ρ_{soil}. The two diurnal soil spectra collected in the study site corresponded to a decline in ρ_{soil} by only 0.04 (Fig. 11A). Although both NDII and NDVI varied as a function of soil wetness, the small diurnal change in soil wetness led to only 0.1% to 0.3% changes in NDII and 0.3% to 0.6% changes in NDVI (Fig. 11B). Thus, our simulations combined with field spectral information provide evidence that the observed changes in MASTER-derived NDII and NDVI were mostly attributed to the diurnal variation in CWC rather than in soil moisture. In addition, the diurnal variation observed with MASTER spectral indexes was consistent with the CWC variation observed in our ground measurements. Furthermore, the weaker influence of soil wetness on NDII and greater sensitivity of NDII to CWC reinforced higher reliability of detected diurnal CWC variation by NDII than by NDVI. Since the influence of soil on diurnal NDII variation was close between two canopy scenarios (Fig. 11B), we are more confident that the higher CWC differences for dense canopies than for sparse canopies (Table 3) resulted from stronger signals from vegetation. Nevertheless, some practical circumstances such as recent rain events and unstable irrigation conditions during the day should be avoided for effective detection of diurnal CWC variation. Considering the challenge of removing the confounding effects of soil and other factors (e.g., sensor noise), this research was not designed to determine the minimum amount of diurnal CWC change that can be detected with airborne remote sensing, but to examine whether a significant change in diurnal CWC observed on the ground could be detected with the MASTER instrument onboard an airborne platform. If the study is successfully scaled up to satellite level using MODIS data, the detection of diurnal CWC variation would benefit greatly from vegetation index achievements in the MODIS community (Cheng et al., 2007; Huete et al., 2002; Trombetti et al., 2008; Zarco-Tejada et al., 2003).

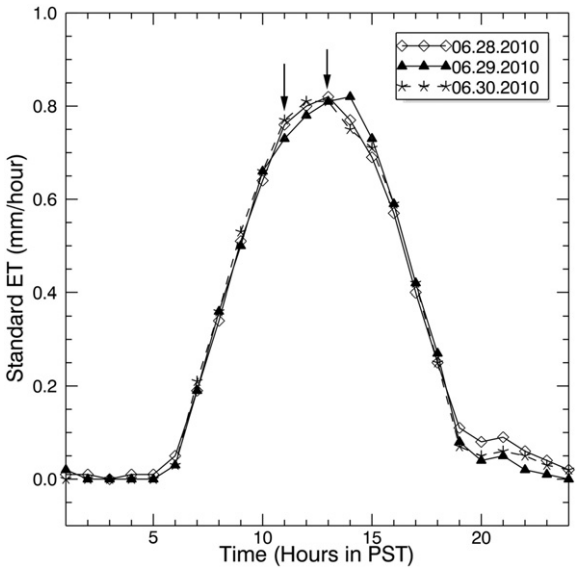

Fig. 10. Diurnal patterns of hourly standard ET data from the closest CIMIS station (CIMIS #146) for the leaf sampling period. Two arrows above the curves denote the times of MASTER flight overpasses.

While aerial remote sensing has been successfully used to quantify seasonal differences in CWC caused by drought stress (Asner et al., 2004), it was unclear whether it could also be used to detect diurnal CWC variation. This study demonstrates the capability of airborne remote sensing for detecting subtle changes in CWC that provide important implications for detecting water deficit at an early stage in both agricultural and natural ecosystems. Our research may be helpful for agricultural management to develop an early warning system of crop water stress using time series of airborne or spaceborne

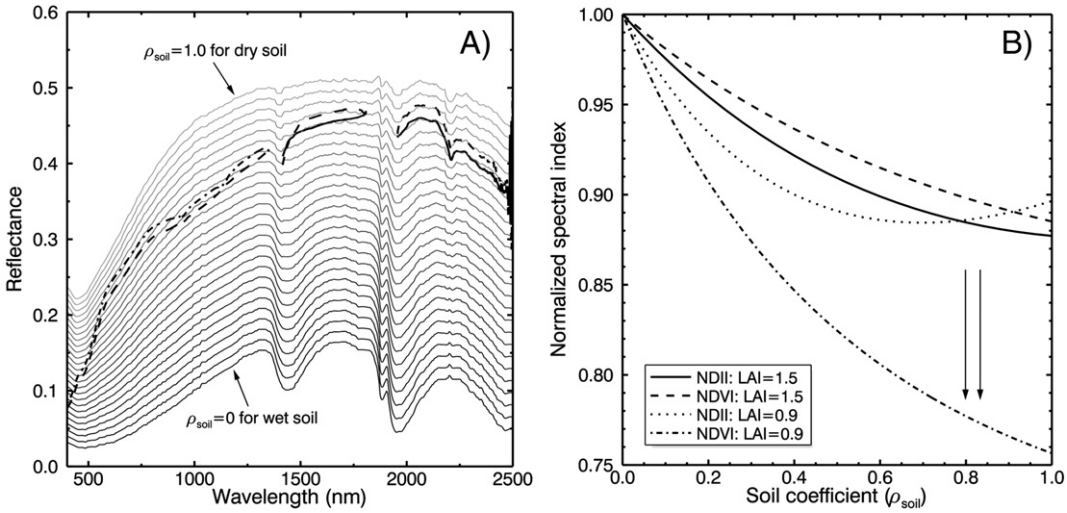

Fig. 11. Soil reflectance spectra for simulations of varying soil moisture, characterized by the soil wetness coefficient ρ_{soil} in the PROSAIL model, in comparison to two diurnal field spectra of bare soil. The soil spectra in gradually brighter color are weighted sums of reflectance spectra from dry soil and wet soil (soil reflectance = $\rho_{soil} \times R_{dry\_soil} + (1 - \rho_{soil}) * R_{wet\_soil}$), with ρ_{soil} values ranging from 0 to 1 in increment of 0.04. The two soil spectra in darker color were collected at the study site in the morning (solid line) and afternoon (dashed line) of June 30, 2011. (B) Effect of variation in soil moisture on spectral indexes NDII and NDVI for two canopy scenarios (LAI = 1.5 for dense canopies and LAI = 0.9 for sparse canopies). NDII and NDVI values were normalized by the values at $\rho_{soil} = 0$. The vertical arrow indicates the approximate soil coefficient positions for the diurnal soil spectra. Fixed parameters for the PROSAIL model were: leaf chlorophyll content = 30 μg/cm^2, carotenoid content = 10 μg/cm^2, equivalent water thickness = 0.016 cm, dry matter content = 0.009 g/cm^2, leaf structure parameter = 1.2, average leaf angle = 50°, hot spot = 0.25, solar zenith angle = 19°, view zenith angle = 0°, relative azimuth angle = 0°, diffuse/direct radiation = 70.

observations. Plant physiologists use plant water potential and relative water content (RWC) as two key metrics of plant water content to characterize water stress (Burghardt & Riederer, 2003; Hunt & Rock, 1989). The two variables are interrelated since zero water potential corresponds to a RWC of 100% (full leaf turgor), which refers to the maximum amount of water a leaf can hold (Nobel, 2009). Because leaves generally do not have full turgor, it is difficult to systematically estimate RWC from canopy reflectance. Therefore, CWC is preferred in the remote sensing community because of its direct relationship with canopy optical properties based on the Beer–Lambert Law and its flexibility for field sampling (Hunt & Rock, 1989; Hunt et al., 1987; Sims & Gamon, 2003).

We chose orchards as the experimental site but our findings could be applied to other agricultural crops and to natural vegetation. Some important ecological studies have shown the usefulness of remote estimates of CWC for detecting forest drought stress (Asner et al., 2004) and mapping the distribution of biological invasion (Asner & Vitousek, 2005; Underwood et al., 2003). Detection of subtle CWC changes would also benefit the prediction of susceptibility to wildfire (Ustin et al., 1998). As an absolute measure of water quantity, CWC can be integrated with water flux data to study water cycling in terrestrial ecosystems. The observed diurnal CWC variation from the aircraft platform also indicates that sub-daily observations of geostationary satellites such as Meteosat (Govaerts & Lattanzio, 2008) from different angles for a specific location may carry detectable spectral changes due to diurnal vegetation activities. Caution should be taken while using the diurnal observations to represent angular observations for studying vegetation dynamics. Future work is needed to investigate the diurnal CWC variation in different seasons and for more vegetation types. This study also opens new research avenues in sub-daily regional mapping of CWC over different ecosystems using high temporal resolution satellite data, such as daily rolling 16-Day MODIS Nadir BRDF-Adjusted Reflectance (NBAR) data (Ju et al., 2010; Shuai, 2010). Since MODIS acquires morning observations from Terra and afternoon observations from Aqua, our findings could be evaluated at the satellite level if the quality of daily rolling data from two separate satellites instead of a combination of both satellites is acceptable.

5. Conclusion

This study provides an evaluation of airborne imagery for detecting diurnal variation in canopy water content over almond and pistachio orchards. A significant decline in CWC (9%) was observed on the ground in response to daily ET in these orchard canopies. We established significant relationships between field-measured CWC and two MASTER-derived simple spectral indexes NDII and NDVI for both morning and afternoon data. The correlations of measured CWC with NDII were stronger than those with NDVI. More importantly, we were able to detect a statistically significant diurnal difference in CWC using both NDII and NDVI. The decline in CWC from morning to afternoon was stronger for sampling blocks with dense canopies than with sparse canopies. However, to achieve this level of accuracy the MASTER imagery had to be corrected for the BRDF effect, especially for diurnal assessment. This research provides useful information for early detection of water stress in crops or other plants with remote sensing data. The strategies for data collection and data processing hold promise for remote detection of diurnal variation in other vegetation physiological variables.

The diurnal CWC maps may serve as remote sensing inputs for the operation of ecosystem models with a sub-daily time step. Our results on the canopy water content could be integrated with evapotranspiration and soil moisture information to aid crop water management and to better understand the water fluxes in agricultural and natural ecosystems.

Acknowledgment

This study was funded by the NASA Terrestrial Hydrology Program (grant # NNX09AN51G) “Multiscale assessment of vegetation water content estimates and its impact on soil moisture for agricultural and natural vegetation”, and USDA Specialty Crop Research Initiative (SCRI project # 0215934) “Advanced sensing and management technologies to optimize resource use in specialty crops”. We thank the NASA SARP program for MASTER data and the field assistance of the 2010 students in that program. We thank field personnel from CSTARS at the University of California, Davis for their assistance

during the field campaign and Dr. Matthias Falk for the assistance with the CIMIS weather data. Thanks to Rose Dominguez and her team for making the MASTER data set available and supporting the atmospheric correction. We are grateful to Paramount Farming Company for supporting the field experiment and allowing us to use their field lab facilities. We would like to thank Lola Suárez and Pablo J. Zarco-Tejada for providing the data in Suárez et al. (2008) for further analysis and valuable feedback on their work in relation to this experiment.

Appendix A. Supplementary data

Supplementary data associated with this article can be found in the online version, at http://dx.doi.org/10.1016/j.rse.2012.12.024. These data include Google maps of the most important areas described in this article.

References

Asner, G. P., Nepstad, D., Cardinot, G., & Ray, D. (2004). Drought stress and carbon uptake in an Amazon forest measured with spaceborne imaging spectroscopy. *Proceedings of the National Academy of Sciences of the United States of America*, *101*, 6039–6044.

Asner, G. P., & Vitousek, P. M. (2005). Remote analysis of biological invasion and biogeochemical change. *Proceedings of the National Academy of Sciences of the United States of America*, *102*, 4383–4386.

Baret, F., Jacquemoud, S., Guyot, G., & Leprieur, C. (1992). Modeled analysis of the biophysical nature of spectral shifts and comparison with information content of broad bands. *Remote Sensing of Environment*, *41*, 133–142.

Beisl, U. (2001). Correction of bidirectional effects in imaging spectrometer data. *Remote Sensing Series*, *37*, University of Zurich: Remote Sensing Laboratories.

Ben-Gal, A., Agam, N., Alchanatis, V., Cohen, Y., Yermiyahu, U., Zipori, I., Presnov, E., Sprintsin, M., & Dag, A. (2009). Evaluating water stress in irrigated olives: Correlation of soil water status, tree water status, and thermal imagery. *Irrigation Science*, *27*, 367–376.

Breda, N., Huc, R., Granier, A., & Dreyer, E. (2006). Temperate forest trees and stands under severe drought: A review of ecophysiological responses, adaptation processes and long-term consequences. *Annals of Forest Science*, *63*, 625–644.

Burghardt, M., & Riederer, M. (2003). Ecophysiological relevance of cuticular transpiration of deciduous and evergreen plants in relation to stomatal closure and leaf water potential. *Journal of Experimental Botany*, *54*, 1941–1949.

Ceccato, P., Flasse, S., & Gregoire, J. M. (2002). Designing a spectral index to estimate vegetation water content from remote sensing data — Part 2. Validation and applications. *Remote Sensing of Environment*, *82*, 198–207.

Ceccato, P., Flasse, S., Tarantola, S., Jacquemoud, S., & Gregoire, J. M. (2001). Detecting vegetation leaf water content using reflectance in the optical domain. *Remote Sensing of Environment*, *77*, 22–33.

Chen, D. Y., Huang, J. F., & Jackson, T. J. (2005). Vegetation water content estimation for corn and soybeans using spectral indices derived from MODIS near- and short-wave infrared bands. *Remote Sensing of Environment*, *98*, 225–236.

Cheng, T., Riaño, D., Koltunov, A., Whiting, M. L., & Ustin, S. L. (2011). Remote detection of water stress in orchard canopies using MODIS/ASTER airborne simulator (MASTER) data. In W. Gao, T. J. Jackson, J. Wang, & N. B. Chang (Eds.), *Remote Sensing and Modeling of Ecosystems for Sustainability VIII, Proceedings of SPIE, Vol. 8156*. http://dx.doi.org/10.1117/12.892889. Bellingham, WA: Society of Photo-Optical Instrumentation Engineers (SPIE).

Cheng, Y. B., Ustin, S. L., Riaño, D., & Vanderbilt, V. C. (2008). Water content estimation from hyperspectral images and MODIS indexes in Southeastern Arizona. *Remote Sensing of Environment*, *112*, 363–374.

Cheng, Y. B., Zarco-Tejada, P. J., Riaño, D., Rueda, C. A., & Ustin, S. L. (2006). Estimating vegetation water content with hyperspectral data for different canopy scenarios: Relationships between AVIRIS and MODIS indexes. *Remote Sensing of Environment*, *105*, 354–366.

Cheng, Y. B., Wharton, S., Ustin, S. L., Zarco-Tejada, P. J., Falk, M., & Paw U, K. T. (2007). Relationships between Moderate Resolution Imaging Spectroradiometer water indexes and tower flux data in an old-growth conifer forest. *Journal of Applied Remote Sensing*, *1*, 013513.

Choudhury, B. J., & Idso, S. B. (1985). Evaluating plant and canopy resistances of field-grown wheat from concurrent diurnal observations of leaf water potential, stomatal-resistance, canopy temperature, and evapotranspiration flux. *Agricultural and Forest Meteorology*, *34*, 67–76.

Chuvieco, E., Riaño, D., Aguado, I., & Cocero, D. (2002). Estimation of fuel moisture content from multitemporal analysis of Landsat Thematic Mapper reflectance data: Applications in fire danger assessment. *International Journal of Remote Sensing*, *23*, 2145–2162.

Colombo, R., Merom, M., Marchesi, A., Busetto, L., Rossini, M., Giardino, C., & Panigada, C. (2008). Estimation of leaf and canopy water content in poplar plantations by means of hyperspectral indices and inverse modeling. *Remote Sensing of Environment*, *112*, 1820–1834.

Davidson, A., Wang, S. S., & Wilmshurst, J. (2006). Remote sensing of grassland–shrubland vegetation water content in the shortwave domain. *International Journal of Applied Earth Observation and Geoinformation*, *8*, 225–236.

Dennison, P. E., & Matheson, D. S. (2011). Comparison of fire temperature and fractional area modeled from SWIR, MIR, and TIR multispectral and SWIR hyperspectral airborne data. *Remote Sensing of Environment*, *115*, 876–886.

Fensholt, R., & Sandholt, I. (2003). Derivation of a shortwave infrared water stress index from MODIS near- and shortwave infrared data in a semiarid environment. *Remote Sensing of Environment*, *87*, 111–121.

Féret, J. B., Francois, C., Asner, G. P., Gitelson, A. A., Martin, R. E., Bidel, L. P. R., Ustin, S. L., le Maire, G., & Jacquemoud, S. (2008). PROSPECT-4 and 5: Advances in the leaf optical properties model separating photosynthetic pigments. *Remote Sensing of Environment*, *112*, 3030–3043.

Friend, A. D., Arneth, A., Kiang, N. Y., Lomas, M., Ogee, J., Rodenbeckk, C., Running, S. W., Santaren, J. D., Sitch, S., Viovy, N., Woodward, F. I., & Zaehle, S. (2007). FLUXNET and modelling the global carbon cycle. *Global Change Biology*, *13*, 610–633.

Galvao, L. S., dos Santos, J. R., Roberts, D. A., Breunig, F. M., Toomey, M., & de Moura, Y. M. (2011). On intra-annual EVI variability in the dry season of tropical forest: A case study with MODIS and hyperspectral data. *Remote Sensing of Environment*, *115*, 2350–2359.

Galvao, L. S., Ponzoni, F. J., Epiphanio, J. C. N., Rudorff, B. F. T., & Formaggio, A. R. (2004). Sun and view angle effects on NDVI determination of land cover types in the Brazilian Amazon region with hyperspectral data. *International Journal of Remote Sensing*, *25*, 1861–1879.

Gao, B. C. (1996). NDWI — A normalized difference water index for remote sensing of vegetation liquid water from space. *Remote Sensing of Environment*, *58*, 257–266.

Govaerts, Y., & Lattanzio, A. (2008). Estimation of surface albedo increase during the eighties Sahel drought from Meteosat observations. *Global and Planetary Change*, *64*, 139–145.

Ham, J. M., Heilman, J. L., & Lascano, R. J. (1990). Determination of soil–water evaporation and transpiration from energy-balance and stem-flow measurements. *Agricultural and Forest Meteorology*, *52*, 287–301.

Hardisky, M. A., Klemas, V., & Smart, R. M. (1983). The influence of soil-salinity, growth form, and leaf moisture on the spectral radiance of spartina-alterniflora canopies. *Photogrammetric Engineering and Remote Sensing*, *49*, 77–83.

Hilker, T., Coops, N. C., Hall, F. G., Black, T. A., Wulder, M. A., Nesic, Z., & Krishnan, P. (2008). Separating physiologically and directionally induced changes in PRI using BRDF models. *Remote Sensing of Environment*, *112*, 2777–2788.

Hook, S. J., Myers, J. E. J., Thome, K. J., Fitzgerald, M., & Kahle, A. B. (2001). The MODIS/ASTER airborne simulator (MASTER) — A new instrument for earth science studies. *Remote Sensing of Environment*, *76*, 93–102.

Houborg, R. M., & Soegaard, H. (2004). Regional simulation of ecosystem CO_2 and water vapor exchange for agricultural land using NOAA AVHRR and Terra MODIS satellite data. Application to Zealand, Denmark. *Remote Sensing of Environment*, *93*, 150–167.

Huete, A., Didan, K., Miura, T., Rodriguez, E. P., Gao, X., & Ferreira, L. G. (2002). Overview of the radiometric and biophysical performance of the MODIS vegetation indices. *Remote Sensing of Environment*, *83*, 195–213.

Hunt, E. R., & Rock, B. N. (1989). Detection of changes in leaf water-content using near-infrared and middle-infrared reflectances. *Remote Sensing of Environment*, *30*, 43–54.

Hunt, E. R., Rock, B. N., & Nobel, P. S. (1987). Measurement of leaf relative water-content by infrared reflectance. *Remote Sensing of Environment*, *22*, 429–435.

Jackson, T. J., Chen, D. Y., Cosh, M., Li, F. Q., Anderson, M., Walthall, C., Doriaswamy, P., & Hunt, E. R. (2004). Vegetation water content mapping using Landsat data derived normalized difference water index for corn and soybeans. *Remote Sensing of Environment*, *92*, 475–482.

Jacquemoud, S., & Baret, F. (1990). PROSPECT: A model of leaf optical properties spectra. *Remote Sensing of Environment*, *34*, 75–91.

Jacquemoud, S., Verhoef, W., Baret, F., Bacour, C., Zarco-Tejada, P. J., Asner, G. P., Francois, C., & Ustin, S. L. (2009). PROSPECT + SAIL models: A review of use for vegetation characterization. *Remote Sensing of Environment*, *113*, S56–S66.

Ju, J. C., Roy, D. P., Shuai, Y. M., & Schaaf, C. (2010). Development of an approach for generation of temporally complete daily nadir MODIS reflectance time series. *Remote Sensing of Environment*, *114*, 1–20.

Jung, M., Reichstein, M., Ciais, P., Seneviratne, S. I., Sheffield, J., Goulden, M. L., Bonan, G., Cescatti, A., Chen, J. Q., de Jeu, R., Dolman, A. J., Eugster, W., Gerten, D., Gianelle, D., Gobron, N., Heinke, J., Kimball, J., Law, B. E., Montagnani, L., Mu, Q. Z., Mueller, B., Oleson, K., Papale, D., Richardson, A. D., Roupsard, O., Running, S., Tomelleri, E., Viovy, N., Weber, U., Williams, C., Wood, E., Zaehle, S., & Zhang, K. (2010). Recent decline in the global land evapotranspiration trend due to limited moisture supply. *Nature*, *467*, 951–954.

Kennedy, R. E., Cohen, W. B., & Takao, G. (1997). Empirical methods to compensate for a view-angle-dependent brightness gradient in AVIRIS imagery. *Remote Sensing of Environment*, *62*, 277–291.

Law, B. E., Falge, E., Gu, L., Baldocchi, D. D., Bakwin, P., Berbigier, P., Davis, K., Dolman, A. J., Falk, M., Fuentes, J. D., Goldstein, A., Granier, A., Grelle, A., Hollinger, D., Janssens, I. A., Jarvis, P., Jensen, N. O., Katul, G., Mahli, Y., Matteucci, G., Meyers, T., Monson, R., Munger, W., Oechel, W., Olson, R., Pilegaard, K., Paw, K. T., Thorgeirsson, H., Valentini, R., Verma, S., Vesala, T., Wilson, K., & Wofsy, S. (2002). Environmental controls over carbon dioxide and water vapor exchange of terrestrial vegetation. *Agricultural and Forest Meteorology*, *113*, 97–120.

Li, P. J., & Moon, W. M. (2004). Land cover classification using MODIS-ASTER airborne simulator (MASTER) data and NDVI: A case study of the Kochang area, Korea. *Canadian Journal of Remote Sensing*, *30*, 123–136.

Los, S. O., North, P. R. J., Grey, W. M. F., & Barnsley, M. J. (2005). A method to convert AVHRR Normalized Difference Vegetation Index time series to a standard viewing and illumination geometry. *Remote Sensing of Environment*, *99*, 400–411.

Matthew, M. W., Adler-Golden, S. M., Berk, A., Felde, G. W., Anderson, G. P., Gorodetzky, D., Paswaters, S., & Shippert, M. (2003). Atmospheric correction of spectral

imagery: evaluation of the FLAASH algorithm with AVIRIS data. In S. S. Shen, & P. E. Lewis (Eds.), *Algorithms and Technologies for Multispectral, Hyperspectral, and Ultraspectral Imagery IX, Proceedings of SPIE*, *Vol. 5093*. http://dx.doi.org/10.1117/12.499604. Bellingham, WA: Society of Photo-Optical Instrumentation Engineers (SPIE).

Meggio, F., Zarco-Tejada, P. J., Miller, J. R., Martin, P., Gonzalez, M. R., & Berjon, A. (2008). Row orientation and viewing geometry effects on row-structured vine crops for chlorophyll content estimation. *Canadian Journal of Remote Sensing*, *34*, 220–234.

Mollot, L. A., Munro, D., & Bilby, R. E. (2007). Classifying fine-scale spatial structure of riparian forests using hyperspectral high-resolution remotely sensed imagery at the Cedar River municipal watershed in western Washington, USA. *Canadian Journal of Remote Sensing*, *33*, 99–108.

Moore, D. S., & McCabe, G. P. (2006). *Introduction to the practice of statistics* (5th ed.). New York: W.H. Freeman and Co (Chapter 14).

Nobel, P. S. (2009). *Physicochemical and environmental plant physiology* (4th ed.). San Diego CA: Academic Press.

Ollinger, S. V. (2011). Sources of variability in canopy reflectance and the convergent properties of plants. *The New Phytologist*, *189*, 375–394.

Peñuelas, J., Filella, I., Biel, C., Serrano, L., & Save, R. (1993). The reflectance at the 950–970 nm region as an indicator of plant water status. *International Journal of Remote Sensing*, *14*, 1887–1905.

R Development Core Team (2010). *R: A language and environment for statistical computing*. Vienna, Austria: R Foundation for Statistical Computing3-900051-07-0.

Reicosky, D. C., Kaspar, T. C., & Taylor, H. M. (1982). Diurnal relationship between evapotranspiration and leaf water potential of field-grown soybeans. *Agronomy Journal*, *74*, 667–673.

Rosa, L. M., & Forseth, I. N. (1996). Diurnal patterns of soybean leaf inclination angles and azimuthal orientation under different levels of ultraviolet-B radiation. *Agricultural and Forest Meteorology*, *78*, 107–119.

Sandmeier, S. R., & Itten, K. I. (1999). A field goniometer system (FIGOS) for acquisition of hyperspectral BRDF data. *IEEE Transactions on Geoscience and Remote Sensing*, *37*, 978–986.

Sauer, T. J., Singer, J. W., Prueger, J. H., DeSutter, T. M., & Hatfield, J. L. (2007). Radiation balance and evaporation partitioning in a narrow-row soybean canopy. *Agricultural and Forest Meteorology*, *145*, 206–214.

Schiefer, S., Hostert, P., & Damm, A. (2006). Correcting brightness gradients in hyperspectral data from urban areas. *Remote Sensing of Environment*, *101*, 25–37.

Sepulcre-Canto, G., Zarco-Tejada, P. J., Jimenez-Munoz, J. C., Sobrino, J. A., de Miguel, E., & Villalobos, F. J. (2006). Detection of water stress in an olive orchard with thermal remote sensing imagery. *Agricultural and Forest Meteorology*, *136*, 31–44.

Serrano, L., Ustin, S. L., Roberts, D. A., Gamon, J. A., & Peñuelas, J. (2000). Deriving water content of chaparral vegetation from AVIRIS data. *Remote Sensing of Environment*, *74*, 570–581.

Shuai, Y. (2010). Tracking daily land surface albedo and reflectance anisotropy with Moderate-resolution Imaging Spectroradiometer (MODIS). PhD Dissertation, Boston University, Boston, Massachusetts, USA.

Simonneau, T., Habib, R., Goutouly, J. P., & Huguet, J. G. (1993). Diurnal changes in stem diameter depend upon variations in water-content: Direct evidence in peach trees. *Journal of Experimental Botany*, *44*, 615–621.

Sims, D. A., & Gamon, J. A. (2003). Estimation of vegetation water content and photosynthetic tissue area from spectral reflectance: A comparison of indices based on liquid water and chlorophyll absorption features. *Remote Sensing of Environment*, *84*, 526–537.

Suárez, L., Zarco-Tejada, P. J., Berni, J. A. J., Gonzalez-Dugo, V., & Fereres, E. (2009). Modelling PRI for water stress detection using radiative transfer models. *Remote Sensing of Environment*, *113*, 730–744.

Suárez, L., Zarco-Tejada, P. J., Sepulcre-Canto, G., Perez-Priego, O., Miller, J. R., Jimenez-Munoz, J. C., & Sobrino, J. (2008). Assessing canopy PRI for water stress detection with diurnal airborne imagery. *Remote Sensing of Environment*, *112*, 560–575.

Trombetti, M., Riaño, D., Rubio, M. A., Cheng, Y. B., & Ustin, S. L. (2008). Multi-temporal vegetation canopy water content retrieval and interpretation using artificial neural networks for the continental USA. *Remote Sensing of Environment*, *112*, 203–215.

Tucker, C. J., Pinzon, J. E., Brown, M. E., Slayback, D. A., Pak, E. W., Mahoney, R., Vermote, E. F., & El Saleous, N. (2005). An extended AVHRR 8-km NDVI dataset compatible with MODIS and SPOT vegetation NDVI data. *International Journal of Remote Sensing*, *26*, 4485–4498.

Underwood, E., Ustin, S., & DiPietro, D. (2003). Mapping nonnative plants using hyperspectral imagery. *Remote Sensing of Environment*, *86*, 150–161.

Ustin, S. L., Roberts, D. A., Pinzon, J., Jacquemoud, S., Gardner, M., Scheer, G., Castaneda, C. M., & Palacios-Orueta, A. (1998). Estimating canopy water content of chaparral shrubs using optical methods. *Remote Sensing of Environment*, *65*, 280–291.

Vanderbilt, V. C., Ustin, S. L., Berger, K. M., Caldwell, W. F., Clark, J. A., Ganapol, B. D., Kasischke, E. S., Martens, S. N., Pettigrew, R. E., & Rousseau, R. A. (1991). Biophysical information in asymmetric and symmetrical diurnal bidirectional canopy reflectance. *IEEE Transactions on Geoscience and Remote Sensing*, *29*, 875–889.

Verhoef, W. (1984). Light-scattering by leaf layers with application to canopy reflectance modeling: the SAIL model. *Remote Sensing of Environment*, *16*, 125–141.

Verhoef, W., Jia, L., Xiao, Q., & Su, Z. (2007). Unified optical-thermal four-stream radiative transfer theory for homogeneous vegetation canopies. *IEEE Transactions on Geoscience and Remote Sensing*, *45*, 1808–1822.

Weber, J. A., & Ustin, S. L. (1991). Diurnal water relations of walnut trees: Implications for remote sensing. *IEEE Transactions on Geoscience and Remote Sensing*, *29*, 864–874.

Wilson, K. B., Baldocchi, D., Falge, E., Aubinet, M., Berbigier, P., Bernhofer, C., Dolman, H., Field, C., Goldstein, A., Granier, A., Hollinger, D., Katul, G., Law, B. E., Meyers, T., Moncrieff, J., Monson, R., Tenhunen, J., Valentini, R., Verma, S., & Wofsy, S. (2003). Diurnal centroid of ecosystem energy and carbon fluxes at FLUXNET sites. *Journal of Geophysical Research-Atmospheres*, *108*(D21). http://dx.doi.org/10.1029/2001JD001349.

Wilson, K., Goldstein, A., Falge, E., Aubinet, M., Baldocchi, D., Berbigier, P., Bernhofer, C., Ceulemans, R., Dolman, H., Field, C., Grelle, A., Ibrom, A., Law, B. E., Kowalski, A., Meyers, T., Moncrieff, J., Monson, R., Oechel, W., Tenhunen, J., Valentini, R., & Verma, S. (2002). Energy balance closure at FLUXNET sites. *Agricultural and Forest Meteorology*, *113*, 223–243.

Yilmaz, M. T., Hunt, E. R., Goins, L. D., Ustin, S. L., Vanderbilt, V. C., & Jackson, T. J. (2008a). Vegetation water content during SMEX04 from ground data and Landsat 5 Thematic Mapper imagery. *Remote Sensing of Environment*, *112*, 350–362.

Yilmaz, M. T., Hunt, E. R., & Jackson, T. J. (2008b). Remote sensing of vegetation water content from equivalent water thickness using satellite imagery. *Remote Sensing of Environment*, *112*, 2514–2522.

Zarco-Tejada, P. J., Rueda, C. A., & Ustin, S. L. (2003). Water content estimation in vegetation with MODIS reflectance data and model inversion methods. *Remote Sensing of Environment*, *85*, 109–124.